Accepted version of

Journal of Physics D: Applied Physics

Low temperature growth study of nano-crystalline TiO2 thin films deposited by RF sputtering

K Safeen, V Micheli, R Bartali, G Gottardi and N Laidani

Published 25 June 2015 • Journal of Physics D: Applied Physics, Volume 48, Number 29

Published version available at: https://iopscience.iop.org/article/10.1088/0022-3727/48/29/295201

DOI: 10.1088/0022-3727/48/29/295201

Influence of intrinsic defects on the electrical and optical properties of TiO_2:Nb films sputtered at room temperature

Kashif Safeen [1,2,3*], V. Micheli[2], R. Bartali[2,3], G. Gottardi[2], Akif Safeen[1], H. Ullah[2,3] and N. Laidani[2]

[1] *Abdul Wali Khan University, Department of Physics, 23200 Mardan, Pakistan*

[2] *Center for Materials and Microsystems, Fondazione Bruno Kessler, Via Sommarive 18, 38123 Povo, Trento, Italy*

[3] *University of Trento, Department of Physics, Via Sommarive 15, 38123 Povo, Trento, Italy*

Abstract

Oxide-based films and nanostructures have emerged as important materials for a wide range of applications such as photovoltaics, optoelectronics, gas sensing and electronics. To develop an appropriate understanding of the properties of these oxides, it is necessary to address the material preparation methods and defect probing issues. This work reports on the synthesis processes of TiO_2 based transparent conductive films, their stoichiometry control and defect identifying, in relation with their electrical and optical properties. Un-doped and TiO_2:Nb films were deposited by RF co-sputtering from TiO_2 and Nb_2O_5 targets in Ar plasma. The chemical species present in the plasmas used in deposition process were investigated by optical emission spectroscopy (OES), which was later on correlated with the defects structure of the films. Analysis by XPS shed more light on the nature of the vacancies and on the effect of the latter on the optical and electrical properties of the films. In terms of results, we measured electrical resistivity in the range 10^{-2}-10^{-3} Ω.cm for the intrinsically and extrinsically doped films (films doped with oxygen

vacancies and Nb^{+5} respectively) while the lowest resistivity was obtained for intrinsically-extrinsically co-doped TiO_2 films (7.4×10^{-4} Ω.cm). The films transparency was also actively determine by the defects in the lattice and highly transparent films (65-85 % in the visible range) were obtained by controlling the density of defects. The approach adopted in this work for the generation of oxygen vacancies could be useful for other oxide-based films, where the oxygen vacancies-dependent properties are crucial, for room temperature ferromagnetism and photocatalytic applications.

Keywords: Transparent conducting oxide; TiO_2 thin films; Sputter deposition; Oxygen vacancies; Electrical properties; Optical properties

Corresponding author: kashifsafeen@awkum.edu.pk (Kashif Safeen)

1. Introduction

Transparent conducting oxides (TCOs) are electrically conductive materials with high transparency in the visible range. TCOs have wide-ranging applications in optoelectrical devices including photovoltaics, displays, opto-electrical interfaces and window glass technologies [1]. The most utilized TCOs are tin-doped indium oxide (ITO), which is suffering from scarcity, poor chemical stability in hydrogen atmosphere and toxicity [2]. Due to these limitations, there is a huge interest to develop alternative TCOs which possess higher conductivity than indium or that use less scarce elements [3]. Currently, many potential candidates are under the extensive study to replace ITO including doped ZnO and SnO_2. However considering the wide ranging application of TCOs, it is necessary to expend the materials range to other non-ITO TCOs.

Epitaxially grown anatase TiO_2 doped by niobium was reported as a new type of TCOs with its room temperature conductivity comparable to that of the commercial ITO based transparent

electrode [4]. Since then many groups have investigated also polycrystalline films and the technology is maturing [5]. The electrical transport properties of the doped TiO_2 films are closely determined by the defects related disorder and the incorporation of foreign impurities [6, 7]. During films growth by sputtering, intrinsic defects (oxygen vacancies) are mostly generated by applying external negative bias at the substrate, which is costly because it needs additional setup for their operation [8]. Furthermore, probably to ensure high transparency, TCOs films are grown in Ar-O_2 plasma [9-11], which is not favorable for oxygen vacancies creation owing to the spontaneous formation of oxygen interstitials (O_{inst}) in O-rich conditions [3]. O_{inst} are predicted to be the detrimental defects for the electrical properties of the films. It not only remove the oxygen vacancies but also form localized shallow acceptor states which compensates the electron doped by Nb^{+5} ions thus depressing the conductivity [12, 13]. Therefore in order to obtained conductive films for such a system, post-growth annealing at high temperature (> 500 °C) is necessary to remove O_{inst} and induced oxygen vacancies, which strongly assisted the films conductivity [12].

In this study, we developed a sample mechanism to control simultaneously the electrical conductivity and optical transparency of TiO_2 films at low temperature (350 °C). We have used the growth pressure parameter to control the energy of the plasma species and hence the density of oxygen vacancies in the growing films. Uniquely, we have deposited the films purely in Ar discharge in which the intrinsic defects generation and the doping is more effective compared with the films deposited in Ar-O_2 plasma. The obtained results can significantly contribute to the development of transparent electrodes by RF sputtering, a suitable technique for coating on large area substrates.

2. Material and methods

2.1 Films deposition

The detailed experimental condition is reported elsewhere [14, 15]. Briefly, TiO_2 and TNO films (TiO_2:Nb) were grown on un-heated p-type silicon (100) and corning glass substrates using radio frequency (13.56 MHz) sputtering in pure Ar discharge. The optimized ceramic TiO_2 (99.9%) having 10 cm of diameter (Materion) and Nb_2O_5 disc (5 cm diameter, ACI Alloys (99.95 % purity) were used as sputtering targets [16]. The total working pressure during the films growth process was varied from 0.8 to 6.6 Pa. A constant dc self-bias on the TiO_2 cathode was maintained at −850 V corresponding to an effective load power of 75 W while power applied to Nb_2O_5 target was fixed at 8 W (self-bias voltage ~ 78 V). The deposition time was adjusted to obtain films having thickness of 85±5 nm. The as-deposited films were annealed in Ar atmosphere (pressure 1.3 Pa) at 350 °C for 1h.

2.2 Plasma diagnostics and films characterization

The discharge properties were studied using Optical Emission Spectroscopy where the plasma light (in the wavelength range 200–850 nm with a spectral resolution of 0.2 nm) was collected with an optical fiber through a quartz window of the sputtering chamber. Subsequently, the light was analyzed by means of a Spectrapro 2300i instrument, equipped with an ICCD camera. The structural properties of the prepared films were characterized by X-ray diffractometer. The measurements were performed by employing CuKα (λ=1.5406 A°) radiation at an incident angle of 3°, in steps of 0.02°, operated at 40 kV and 30 mA (Italstructures APD2000). The average crystallite sizes of anatase were calculated from the broadening of X-ray diffraction peaks (101) using the Scherrer's formula ($D = 0.9\lambda/B cos\theta$) [17]. The thicknesses of the films were

estimated using a surface profiler (Tencor Instruments). TiO_2 films chemical properties were analyzed with a Scienta ESCA 200 spectrometer with a monochromatic Al Kα x-ray source (1486.6 eV). The spectra of C1s, O1s, Ti2p and Nb3d core lines were acquired at 150 eV pass energy (resolution of 0.4 eV). Data reduction was made using homemade software based on R platform [18]. A double beam spectrophotometer (Model–JASCO V-670), single monochromator design covering a wavelength range of 200 to 2800 nm was employed to record the optical transmittance of the deposited films at normal light incidence. The optical band gap of prepared films was estimated using Tauc model. The resistivities of the obtained films were measured by van der Pauw method and the carrier density and their mobility was determined by Hall Effect measurements using RH 2030 PhysTech instrument.

3. Results and discussions

3.1 Plasma Properties

The optical emission spectrum was acquired from 200 to 850 nm where many emission peaks related to Ar, Ar^+, Ti, and Ti^+ were observed (the detail of these characteristic emission lines is reported in [7, 14]). Fig. 1 (a) illustrates the optical emission spectra of the films prepared at lowest (0.8 Pa) and highest pressures (6.6 Pa). We observed that the population of excited plasma species (Ar, Ar^+, Ti, Ti^+) was greater at highest working pressure.

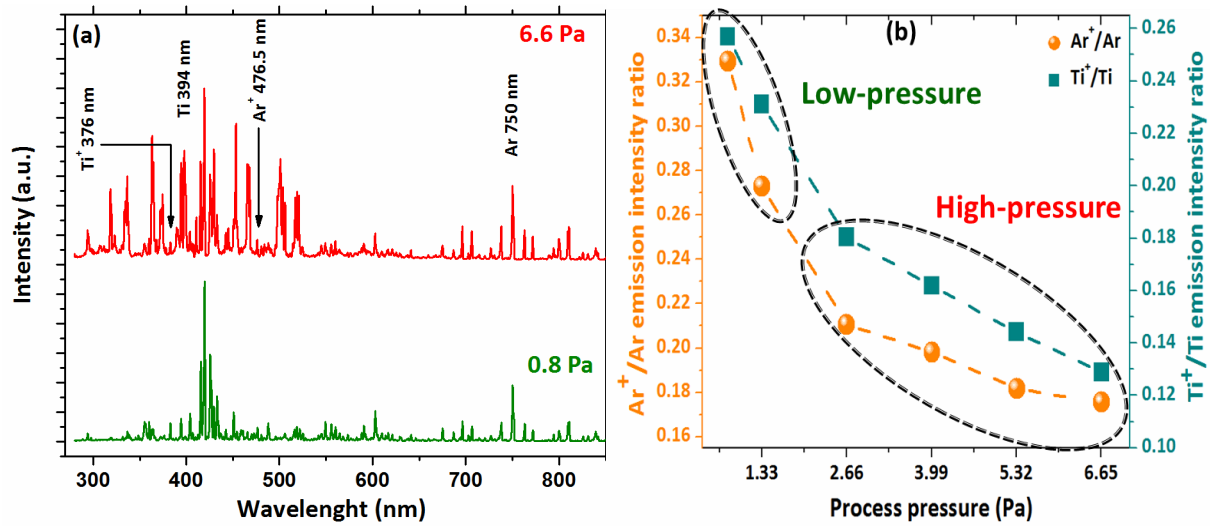

Fig. 1: (a) Optical emission spectrum from RF sputtering discharge of Nb_2O_5 and TiO_2 target in Ar (b) Variation of Ar^+/Ar and Ti^+/Ti emission intensity ratios as a function of discharge pressure.

To gain more insight into the plasma characteristics for the present work, the relative concentration of the positive ions was estimated using the emission intensity ratios Ar^+/Ar and Ti^+/Ti (Fig. 1 (b)). The Figure reveals that the spectral line intensity ratio of Ar^+/Ar and Ti^+/Ti is clearly increasing with decreasing the total pressure for the whole process pressure range. A more close inspection of the Figure enables us to identify two regions of the emission intensity behavior. Firstly, increment of Ar^+/Ar and Ti^+/Ti emission intensity ratios with reducing the growth pressure is minimal until 2.66 Pa (i.e. from 0.18 to 0.21), let's call it "high process pressure regime". In the second region, which is known as "low process pressure state", the relative population of the positive ions increases significantly (from 0.21 to 0.33) with dropping the process pressure. Notably, the low process pressure regime consisted of only two points (1.33 and 0.8 Pa) but their effect is remarkable on the electrical and optical properties of the films, as discussed in the sections 3.4 and 3.5. This indicates that the ionization degree of Ar and Ti rises

with a decrease in the working pressure. This behavior may be explained by the fact that by decreasing the total pressure, the mean free path of electrons is enlarged. Consequently, the electrons undergo less-frequent collisions with plasma species which increases the electronic temperature leading to more-efficient ionization of Ar and Ti.

The influence of total pressure on the energy and density of electrons and ions is also reported previously. For instance, Kubota *et al.* [19] systemically studied the behavior of (V_p-V_{fl}) for different process pressures using Langmuir probe technique, where V_p is the plasma potential and V_{fl} represent the floating potential which is negative due to the higher electrons mobilities as reported in [8] (V_{fl}∼-35 V) and [19] (V_{fl}∼-15 V). The value of "(V_p-V_{fl})" was estimated to be 78 V and 27 V for the gas pressure of 8.9×10^{-3} Pa and 2.5×10^{-2} Pa respectively (with V_{fl}∼-15 V). They concluded that ion energy at lowest pressure is higher than the high pressure. Similarly it was reported that the ionization of Ar increases with decreasing the working pressure from 120 to 2 mTorr due to longer electron mean free path and higher energy [20]. Furthermore, the Ar ions detected by electrostatic energy analyzer at 2 mTorr pressure has higher kinetic energy (36 eV) compared to 20 mTorr where Ar^+ possess energy around 26 eV [20]. Likewise, Klaus Ellmer work on transparent and conductive ZnO films shows that ions in the rf discharge possess higher energies with a substrate at floating potential. The rf energy distribution exhibits a saddle-like broad shape with Ar^+ energy in the range 20-45 eV [21]. Since we also performed experiments with substrate at V_{fl}, therefore we expect that positive ions become more energetic with reducing the pressure which is well-supported by the increasing Ar^+/Ar and Ti^+/Ti emission intensity ratio.

3.2 Chemical Properties of the Films

To determine the effect of energetic ions bombardment on the films chemical properties, X-ray photoelectron spectroscopy (XPS) measurements were performed. The O1s XPS spectrum of

TNO films deposited in Ar plasma is presented in Fig. 2 (a) where the peaks are de-convoluted into two peaks centered at 530.91 eV (Component I, OI) and 532.13eV (component II, OII). The lower binding energy peak can be attributed to the oxygen bound to Ti^{+4} and Nb^{+5} in TiO_2:Nb whereas the higher binding energy component may arises due to the oxygen contribution in the Ti–OH bonds, possible C–O–C, C–OH groups and also oxygen in the Ti_2O_3 phase contribution [22]. Fig. 2 (b) shows the Ti2p core-level spectra of the as-grown TNO films deposited at 2.6, 1.3 and 0.8 Pa, where 2.6 Pa is the representative of the high process pressure values (4, 5.3 and 6.6 Pa). For high process pressure ($\geq$ 2.6 Pa), the BE (binding energy) of $Ti2p_{3/2}$ and $Ti2p_{1/2}$ spin-orbit components are located at 459.31 and 465.04 eV respectively which indicates that the oxidation state of Ti is +4. No shoulder peak at lower binding energy side is evident implying that the films are less oxygen-deficient (Ti^{+3}/Ti^{+4}~0). For 1.3 Pa, a low intensity shoulder peak at 457.68 eV corresponding to Ti^{+3} states appeared which indicates the transition from less oxygen-deficient to more oxygen-deficient films (Ti^{+3}/Ti^{+4}~0.032). More significantly, the Ti^{+3} signals become more prominent for process pressure of 0.8 Pa (Ti^{+3}/Ti^{+4}~0.079). This can be explained by the fact that decreasing the process pressure, Ar^{+} and Ti^{+} ions become more energetic as discussed in section 3.1. The bombardment of high kinetic energy ions (Ar^{+} and Ti^{+}) on the growing films remove the lattice oxygen in TiO_2 and creates oxygen vacancies. The electrons trapped in oxygen vacancy form two reduced Ti^{3+} cations according to Ti^{+4}-O^{-2}-Ti^{+4} $\rightarrow$ Ti^{+3}-□-Ti^{+3}+1/2O_2 [23]. Further, for the prepared films, the oxide stoichiometry, Nb concentration in TiO_2 films and various atomic ratios were also estimated from the XPS analysis (see Table 1). On the basis of the Ti^{+3}/Ti^{+4} atomic ratio values, the electrical and optical properties of the films are discussed in section in 3.4 and 3.5.

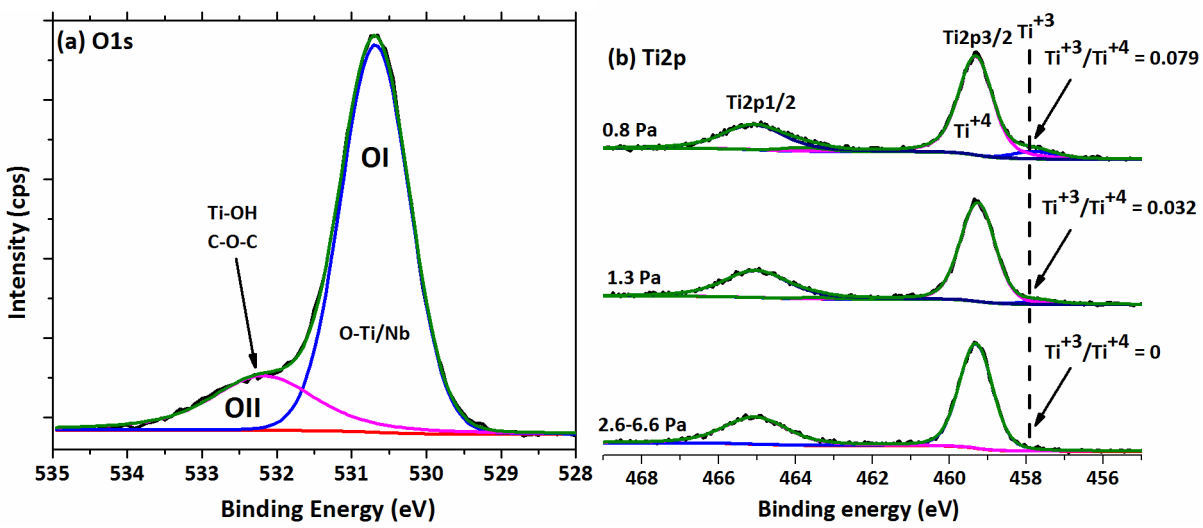

Fig. 2: (a) O1s core-level of the films grown at 1.3 Pa (b) XPS Ti2p core level for the TNO films grown at 2.6, 1.3 and 0.8 Pa

Table 1: Nb concentation and Ti^{+3}/Ti^{+4} atomic ratios for different discharge pressure values; the as-deposited and annealed films are represented as "A.D." and "A.A." respectively

Pressure (Pa)	Nb at.%	O_I/Nb+Ti	Ti^{+3}/Ti^{+4} (A.D.)	Ti^{+3}/Ti^{+4} (A.A.)
0.8	6.88	1.75	0.079	0.11
1.3	6.92	1.72	0.032	0.039
2.6	5.52	1.80	0	0
4	5.02	1.81	0	0
5.3	4.84	1.77	0	0
6.6	3.56	1.78	0	0

3.3 Structural Properties of the Films

The XRD results show that the TNO films deposited on un-heated substrate have amorphous nature, regardless of the process pressures (not shown here). The amorphous films were subsequently annealed at 350 °C to obtain the crystalline phase and to activate Nb doping. In the XRD spectra, the strongest intensity of the (101) diffraction peak around 25.20° indicates a preferred oriented anatase polycrystalline structure for all the growth pressure values except for process pressure of 0.8 Pa, for which the TNO films remained amorphous (Fig. 3). The peaks associated to the (004) and (200) crystallographic planes were also observed, although of weak intensity. No other extra peak corresponding to rutile or niobium oxide phase was evident from the XRD profile. The persistence of amorphous phase after annealing for the film grown at a process pressure of 0.8 Pa could be due to the structural damage in the film due to the interaction of high energetic positive ions (Ar^{+} and Ti^{+}) with the films. Our assumption is well-supported by the OES, XPS results and films deposition rate where higher Ar^{+}/Ar emission intensity ratio (0.33), greater Ti^{+3}/Ti^{+4} atomic ratio (0.079), the presence of Nb^{+4} chemical state and the lower deposition rate (high anti-sputtering phenomenon) was observed for the films grown at process pressure of 0.8 Pa compared to the films deposited at process pressure ≥ 1.3 Pa. Moreover for the pressure range (1.3-6.6 Pa), the crystallite size value of Nb-doped TiO_2 films (~26-28 nm) is comparable to the un-doped TiO_2 films (27.30±0.3 nm) indicating that Nb incorporations in TiO_2 does not affect its crystallite size.

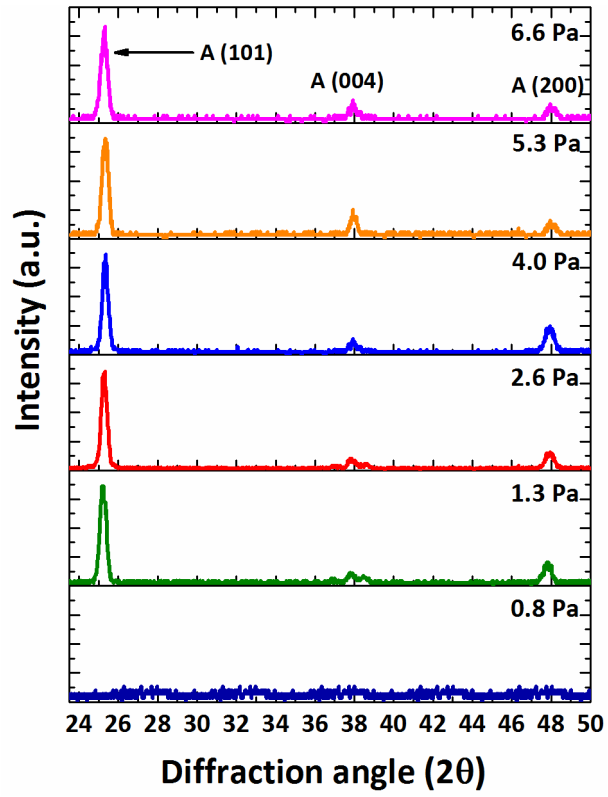

Fig. 3: XRD patterns of the annealed TNO films at 350 °C in argon for various deposition process pressure values

3.4 Electrical Properties of the Films

3.4.1 Influence of intrinsic defects on the resistivity of as-grown TiO_2:Nb samples

In Figure 4, the blue solid squares and the red triangular symbol headed up represent the defects density-dependent resistivity values of TNO and TiO_2 films prepared at room temperature. The as-deposited films grown at high process pressure (≥ 2.6) Pa were insulating ($\rho \sim 10^7$ Ω.cm). This result is consistent with the XPS observation where no shoulder peak in the Ti2p core-level corresponding to Ti^{+3} states was detected (Ti^{+3}/Ti^{+4} atomic ratios ~ 0, for four samples). More significantly, in the low pressure regime (≤ 1.3 Pa), the resistivity dropped enormously to < 10 Ω.cm, almost by 10^6-fold compared with the films prepared at pressure ≥ 2.6 Pa ($\rho \sim 10^7$ Ω.cm),

which is explained by the presence of oxygen vacancies in the films (Ti^{+3}/Ti^{+4} atomic ratios ~ 0.032-0.079). This result is significant because the films which were semiconductive in the as-grown form were conductive after annealing. It is important to note that Nb is not activated as a donor in the as-deposited TNO samples and the semiconducting behavior is solely attributed to the oxygen vacancies induced donor states.

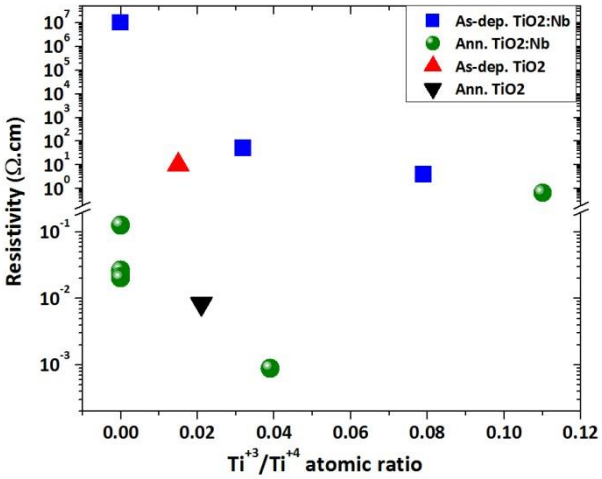

Fig. 4: Comparison of the resistivity values of the as-prepared and annealed TiO_2 and TNO films for different Ti^{+3}/Ti^{+4} XPS atomic ratios

3.4.2 Effect of annealing on the electrical properties of TiO_2:Nb samples

Thermal annealing was performed in Ar atmosphere at 350 °C to crystallize the films and to activate Nb doping in TiO_2 matrix. The crystallization process substantially improved the conductivity of TNO films as shown in Fig. 4 and Table 2. The resistivity values of TNO films deposited at process pressure of ≥ 2.6 Pa, which corresponds to Ti^{+3}/Ti^{+4} atomic ratios ~ 0, decreased from 10^7 to 10^{-1}-10^{-2} Ω.cm after heat treatment (represented by the green solid circles in Fig. 4). The 10^8-fold drop in resistivity values after annealing indicates the substitution of Nb^{+5} ions for Ti^{+4} site in TiO_2 lattice (n-type doping). The resistivity of the samples deposited at

1.3 Pa (Ti^{+3}/Ti^{+4} atomic ratios ~ 0.039), which was already semiconductive in the as-grown form, dropped significantly to 7.45×10^{-4} Ω.cm with thermal annealing. The minimum resistivity corresponds to an electron carrier density of 5.54×10^{21} cm^{-3} and carrier mobility of 1.51 $cm^2/V.s$. Notably, the resistivity of the films grown at process pressure of 0.8 Pa did not reduce considerably from 0.98 Ω.cm with the heat treatment (Ti^{+3}/Ti^{+4} atomic ratios ~ 0.11). From a structural prospective, this may be attributed to the detrimental effect of ion bombardment on the films which damage the films quality and inhibited the amorphous-to-anatase phase transformation. Interestingly, the un-doped TiO_2 films deposited with a process pressure of 1.3 Pa and subsequently annealed at 350 °C exhibited a resistivity of the orders of 8.4×10^{-3} Ω.cm, solely due to the ionization of oxygen vacancies (see the black triangular symbols headed down in Fig. 4).

Table 2: Film thickness, electron carrier concentration (n_e), Hall mobility (μ_H), resistivity (ρ) and sheet resistance (R_s) values of the TNO films deposited at different total pressure (P_t) and annealed at 350 °C in argon

P_t (Pa)	Thickness (nm)	n_e (cm^{-3})	μ ($cm^2.V^{-1}.s^{-1}$)	ρ (Ω.cm)	R_s (Ω/sq.)
TNO 0.8	**87.2±11.8**	**6.75×10^{17}**	**14.9**	**6.610×10^{-1}**	**7.78×10^{4}**
TNO 1.3	**85.4±7.6**	**5.54×10^{21}**	**1.51**	**7.45×10^{-4}**	**106**
TNO 2.6	**85.2±14.4**	**3.42×10^{20}**	**0.90**	**2.02×10^{-2}**	**2.44×10^{3}**
TNO 4.0	**89.2±7.4**	**9.09×10^{20}**	**0.32**	**2.15×10^{-2}**	**2.22×10^{3}**
TNO 5.3	**87.9±6.9**	**3.80×10^{20}**	**0.62**	**2.66×10^{-2}**	**3.02×10^{3}**
TNO 6.6	**81.1± 10.7**	**7.67×10^{20}**	**0.065**	**1.26×10^{-1}**	**1.56×10^{4}**
TiO_2 (1.3)	**84.3±6.3**	**2.23×10^{20}**	**3.4**	**8.39×10^{-3}**	**987**

3.4.3 Discussions

Fig. 5 shows a general representation of the doping process used in this work. Briefly, it is known that free carriers in TNO system are contributed by two principal donors: Nb^{+5} substituting in the crystalline lattice for Ti^{+4} and charged oxygen vacancies (F^{+} and F^{++} centers). The latter is called intrinsic doping while the former is known as extrinsic doping. We considered all the annealed TNO films made at pressure ≥ 2.6 Pa as extrinsically-doped films (with Nb^{+5}) because we did not observe any evidence of oxygen vacancies by XPS analysis and the electrical results of the as-deposited samples (Ti^{+3}/Ti^{+4} atomic ratios ~ 0 and films were electrically insulating). In this case, a maximum electron carrier density of 3.42×10^{20} cm^{-3} was observed which corresponds to a resistivity value of 2.02×10^{-2} Ω.cm. For intrinsic doping in TiO_2, the n-type conductivity was due to the ionization of oxygen vacancies. In this case, a minimum resistivity of 8.39×10^{-3} Ω.cm was measured with a carrier density of 2.23×10^{20} cm^{-3} and mobility value around 3.4 $cm^2V^{-1}s^{-1}$. In contrast, for the most conductive TNO films deposited at pressure of 1.3 Pa, oxygen vacancies presence was established in XPS and electrical measurement. During the thermal annealing not only Nb^{+5} is substituted for Ti^{+4} donating electrons but also the electron loosely bound to F centers delocalized to the conduction band, thus increasing the carrier density to 5.54×10^{21} cm^{-3}. This is called intrinsic–extrinsic doping in TiO_2 (V_o+Nb). Therefore the lowest resistivity value (7.45×10^{-4} Ω.cm) compared to the films deposited at pressure ≥ 2.6 Pa (2.02×10^{-2} Ω.cm) could be due to the contribution of both the oxygen vacancies and extrinsic dopants to the conductivity of the films. The lowest resistivity obtained in this work (7.45×10^{-4} Ω.cm) is 3-fold higher than the epitaxially grown TNO films on single crystalline $LaAlO_3$ and $SrTiO_3$ substrate at 600 °C [4], knowing that our films were grown at room temperature and annealed at low temperature (350 °C). The resistivity value of the

prepared films is lower than reported in [10] ($\rho = 1\times10^{-3}$ Ω.cm, annealing temperature: 600 °C), [24] ($\rho = 9.2\times10^{-4}$ Ω.cm, annealing temperature: 600 °C) and [25] ($\rho = 1.1\times10^{-3}$ Ω.cm, annealing temperature: 600-800 °C).

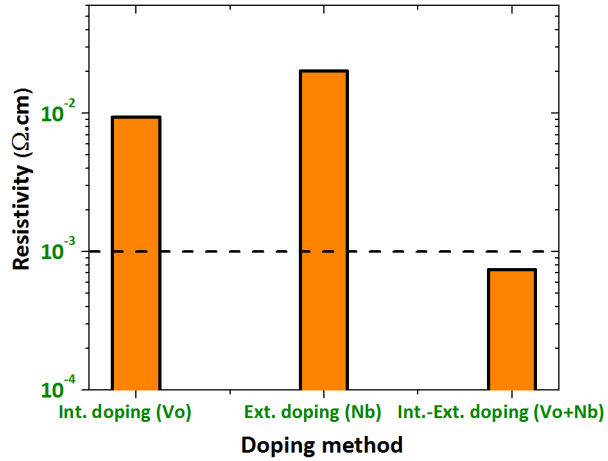

Fig. 5: An illustration of the method used for doping in TiO_2, V_o indicates doping by oxygen vacancies (Int. doping), Nb represent doping by Nb (Ext. doping) and V_o+Nb shows Int.-Ext. doping in TiO_2

It is important to mention that the plasma (Ar discharge) used in this work is effective for the synthesis of transparent-conductive films at low temperature compared with the work reported in huge amount of literature, where the films were grown in Ar-O_2 discharge [11, 26, 27]. In the latter case, the films transparency is usually high due to the lack of oxygen vacancies. However, sputtering in Ar-O_2 plasma leads to O_{inst} in the films, which is not supportive for the films conductivity because: (i) it filled up the oxygen vacancies (ii) it compensated the electron donated by Nb [10]. Therefore, both these phenomenons resulted in the growth of high resistive films. In such case, the key role of post-growth annealing in reduced environment to enhance the conductivity is therefore mainly to drive out O_{ints} from the lattice so as to suppress this charge compensation channel [10]. Mattheiss *et al.* reported that generation of the oxygen vacancies can

be enhanced by increasing the annealing temperature because the oxygen vacancies formation is endothermic [28]. However, higher annealing temperature (550-800 °C) as reported in [25-27] is not cost-effective (more energy consumption, use for the quartz substrates, not feasible for the plastic substrates etc.). Therefore, we propose to grow the films in Ar discharge instead of Ar-O_2 plasma. In this way, one can control the formation of O_{int} and can easily induce oxygen vacancies in the films (using the energetic of the species involve in the deposition process, as demonstrated in our work), which is useful for the synthesis of transparent-conductive films at low temperature (~ 350 °C).

3.5 Optical Properties of the Films

Fig. 6 (a) compares the average visible transparency (T_{VIS}) of the films before and after annealing with the density of oxygen vacancies (Ti^{+3}/Ti^{+4} atomic ratios). Fig. 6 (b) illustrates the optical transmittance spectrum of the annealed TNO films in the wavelength range 200-2800 nm for various process pressure values. As evident from Fig 6 (a), the films grown at pressure ≥ 2.6 Pa exhibited T_{VIS} > 80% which could be explained by the fact that these films contain less density of oxygen vacancy defects as no Ti^{+3} shoulder peak in the Ti2p core-level was detected in Ti2p spectra (Ti^{+3}/Ti^{+4}=0, see the solid blue squares in Fig. 6 (a)). Notably, the mean transmittance in the visible range dropped to 70% at process pressure = 1.3 Pa (Ti^{+3}/Ti^{+4}∼0.032). The low transmittance or light absorption may be due to the deep oxygen vacancy states which is even more noticeable at lowest pressure (0.8 Pa) where T_{VIS} is only 60% (Ti^{+3}/Ti^{+4}∼0.079). It is important to mention here that annealing process improved the films transparency for all the growth pressure values. For the TNO films which show the best electrical properties (ρ = 7.45×10^{-4} Ω.cm), the average visible transparency increased from 70 to 77 % after thermal annealing. The improvement in the transmittance by thermal annealing is attributed to the

ionization of neutral and singly ionized oxygen vacancies to doubly ionized oxygen vacancies (F^{++} center) which is optically silent as it does not hold electrons [29]. The films densification and reduction in the pores after annealing might also be the reason for the increased in transmittance. Further, due to high n_e (5.54×10^{21} cm^{-3}), the most conductive films displayed a low transmittance in the NIR due to the plasma oscillations (Fig. 6 (b)). In contrast the films with $n_e \sim 3.42\times10^{20}$ cm^{-3} have relatively high transparency in the NIR region. Our work indicates that high transparent films can be obtained by controlling the density of defects without using Ar-O_2 as a sputtering discharge, which is not appropriate for the electrical transport properties of TiO_2 films.

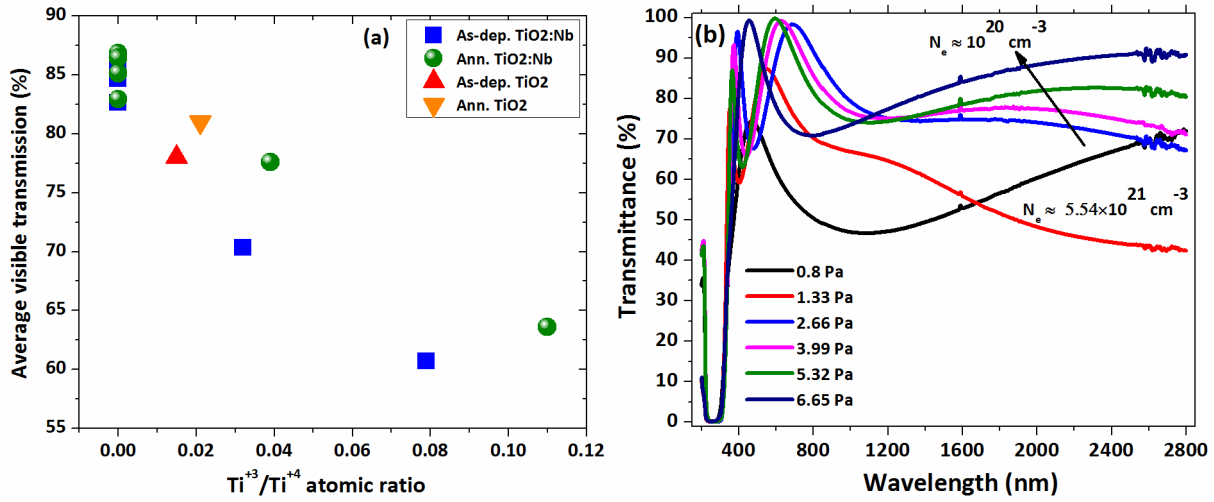

Fig. 6: (a) Variation of the average transmittance with Ti^{+3}/Ti^{+4} atomic ratios deduced from XPS (b) optical transmittance of TNO films annnealed in argon at 350 °C

The optical band gap (E_{OPT}) of as-prepared and annealed films in argon was estimated using Tauc model. The E_{OPT} the as-deposited films prepared at various pressures was in the range 3.21-3.26 eV. Generally after annealing, fundamental absorption energy values shift towards higher energies with Nb doping (except for process pressure = 0.8 Pa) but the blue shift was more

significant for the intrinsically-extrinsically co-doped TiO_2 films. In this case, we estimated an increment in the band gap of the doped TiO_2 films by ~0.22 eV compared with the as-grown film (3.25 eV). This shift may be attributed to the well-known Burstein–Moss effect, usually observed in degenerate semiconductors, where the transition occurs from the filled band to the lowest unfilled level in the conduction band [30-32]. Castro et al. estimated an increment in the band gap of TNO films by ~0.25 eV compared with the bulk anatase (3.20 eV) [33]. Zhang et al. also have found an increase in the band-gap from 3.22 eV for TiO_2 to 3.37 eV for 5% Nb doped TiO_2 film [34]. It is important to mention here that the blue shift in the absorption edge is not due to the quantum confinement effect; because in the present case the crystallite size is larger (~26-28 nm) than necessary for the quantum size effect (< 10 nm) [35]. For the films grown at lowest pressure (0.8 Pa), the E_{OPT} of the as-grown and annealed film is comparable indicating the ineffectiveness of the dopants, consistence with electrical and XRD results.

Under the application point of view, the prepared films exhibited sheet resistance around 106 Ω/sq. with transmissivity greater than 85% at 550 nm, which meets the requirement for flat panel displays and touch screen applications. It can also fulfill the need of functional glasses such as electrochromic and low-emissivity glass windows. Moreover, by adjusting the growth pressure, we can produce highly transparent films (T_{VIS} > 85%) with modest resistivity (R_s ~ 2000 Ω/sq.) which is suitable for electromagnetic shielding applications, for example for cathode-ray tubes used for video display terminals.

3.6 Conclusion:

We demonstrated how to control the electrical conductivity and optical transparency of the doped TiO_2 films at low temperature (350 °C). We explored three doping methods i.e. intrinsic,

extrinsic and intrinsic-extrinsic co-doping in TiO_2 by varying the process pressure (from 0.8 to 6.65 Pa). Primarily, emphasis was put on the generation of intrinsic defects using energetic of the species involved in the process and investigated its influence on the electrical and optical properties of the films. We observed that the bombardment of high energetic species onto the films at low process pressure (≤ 1.3 Pa) induced intrinsic defects in the lattice. Consequently, the as-grown films exhibited semiconducting behavior having resistivity < 10 Ω.cm. After thermal annealing at 350 °C, the intrinsic-extrinsic co-doping method was found the most effective route of doping where the lowest resistivity of 7.45×10^{-4} Ω.cm was obtained compared with the single intrinsic or extrinsic doping ($\rho \sim 10^{-2}$-10^{-3} Ω.cm). The optical properties of the films also strongly depend on the defects in the films and highly transparent films can be obtained by controlling the intrinsic defects.

References:

[1] A. Stadler, Transparent conducting oxides—An up-to-date overview, Materials 5(4) (2012) 661-683.
[2] T. Hitosugi, N. Yamada, S. Nakao, Y. Hirose, T. Hasegawa, Properties of TiO2-based transparent conducting oxides, physica status solidi (a) 207(7) (2010) 1529-1537.
[3] H.-Y. Lee, J. Robertson, Doping and compensation in Nb-doped anatase and rutile TiO2, Journal of Applied Physics 113(21) (2013) 213706.
[4] Y. Furubayashi, T. Hitosugi, Y. Yamamoto, K. Inaba, G. Kinoda, Y. Hirose, T. Shimada, T. Hasegawa, A transparent metal: Nb-doped anatase TiO[sub 2], Applied Physics Letters 86(25) (2005) 252101.
[5] H.A. Huy, B. Aradi, T. Frauenheim, P. Deák, Comparison of Nb-and Ta-doping of anatase TiO2 for transparent conductor applications, Journal of Applied Physics 112(1) (2012) 016103.
[6] L. Sheppard, T. Bak, J. Nowotny, M. Nowotny, Effect of oxygen activity on niobium segregation in niobium-doped titanium dioxide, Journal of the Australian Ceramic Society 44(2) (2008) 42.
[7] M.K. Safeen, Growth Study and Characterization of TiO2 Based Thin Films for Low Temperature Synthesis of Transparent Conductive Films, University of Trento, 2016.
[8] B.K. Sarma, A.R. Pal, H. Bailung, J. Chutia, Role of ion energy on growth and optical dispersion of nanocrystalline TiO2 films prepared by magnetron sputtering with ion assistance at the substrate, Applied Surface Science 258(15) (2012) 5659-5665.
[9] N. Yamada, T. Hitosugi, J. Kasai, N.L.H. Hoang, S. Nakao, Y. Hirose, T. Shimada, T. Hasegawa, Direct growth of transparent conducting Nb-doped anatase TiO[sub 2] polycrystalline films on glass, Journal of Applied Physics 105(12) (2009) 123702.

[10] T. Junguang, H. Pan, W. Lai Mun, W. Ten It, J.W. Chai, P. Jisheng, S.J. Wang, Mechanism of insulator-to-metal transition in heavily Nb doped anatase TiO 2, Materials Research Express 1(1) (2014) 015911.
[11] N. Yamada, T. Hitosugi, N.L.H. Hoang, Y. Furubayashi, Y. Hirose, S. Konuma, T. Shimada, T. Hasegawa, Structural, electrical and optical properties of sputter-deposited Nb-doped TiO2 (TNO) polycrystalline films, Thin Solid Films 516(17) (2008) 5754-5757.
[12] J. Tao, H. Pan, L.M. Wong, T.I. Wong, J. Chai, J. Pan, S. Wang, Mechanism of insulator-to-metal transition in heavily Nb doped anatase TiO2, Materials Research Express 1(1) (2014) 015911.
[13] H. Nogawa, A. Chikamatsu, Y. Hirose, S. Nakao, H. Kumigashira, M. Oshima, T. Hasegawa, Carrier compensation mechanism in heavily Nb-doped anatase Ti 1− x Nb x O 2+δ epitaxial thin films, Journal of Physics D: Applied Physics 44(36) (2011) 365404.
[14] K. Safeen, V. Micheli, R. Bartali, G. Gottardi, N. Laidani, Low temperature growth study of nano-crystalline TiO2thin films deposited by RF sputtering, Journal of Physics D: Applied Physics 48(29) (2015) 295201.
[15] R. Bartali, V. Micheli, G. Gottardi, A. Vaccari, M.K. Safeen, N. Laidani, Nano-hardness estimation by means of Ar+ ion etching, Thin Solid Films 589 (2015) 376-380.
[16] K. Safeen, V. Micheli, R. Bartali, G. Gottardi, A. Safeen, H. Ullah, N. Laidani, Synthesis of conductive and transparent Nb-doped TiO2 films: Role of the target material and sputtering gas composition, Materials Science in Semiconductor Processing 66 (2017) 74-80.
[17] W.H. Shah, K. Safeen, G. Rehman, Effects of divalent alkaline earth ions on the magnetic and transport features of La 0.65 A 0.35 Mn 0.95 Fe 0.05 O 3 (A= Ca, Sr, Pb, Ba) compounds, Current Applied Physics 12(3) (2012) 742-747.
[18] R.C. Giorgio Speranza, RxpsG free software for XPS data processing, Fondazione Bruno Kessler - Trento, 2016.
[19] E. Kubota, Y. Shigesato, M. Igarashi, T. Haranou, K. Suzuki, Effects of magnetic field gradient on crystallographic properties in tin-doped indium oxide films deposited by electron cyclotron resonance plasma sputtering, Japanese Journal of Applied Physics 33(9R) (1994) 4997.
[20] Kunio Okimura, Akira Shibata, Mass and Energy Analyses of Substrate-incident Ions in TiO 2 Deposition by RF Magnetron Sputtering, Japanese Journal of Applied Physics 36(1R) (1997) 313.
[21] K. Ellmer, T. Welzel, Reactive magnetron sputtering of transparent conductive oxide thin films: Role of energetic particle (ion) bombardment, Journal of Materials Research 27(05) (2012) 765-779.
[22] I. Luciu, R. Bartali, N. Laidani, Influence of hydrogen addition to an Ar plasma on the structural properties of TiO2−xthin films deposited by RF sputtering, Journal of Physics D: Applied Physics 45(34) (2012) 345302.
[23] Z. Xi-Song, L. Yuan-Hua, L. Bo, L. Ling-Jia, Z. Jian-Ping, N. Ce-Wen, Processing and characterization of TiO 2 film prepared on glass via pulsed laser deposition, Journal of Physics D: Applied Physics 39(3) (2006) 558.
[24] K.-H. Hung, P.-W. Lee, W.-C. Hsu, H.C. Hsing, H.-T. Chang, M.-S. Wong, Transparent conducting oxide films of heavily Nb-doped titania by reactive co-sputtering, Journal of Alloys and Compounds 509(42) (2011) 10190-10194.
[25] X.W. Zheng, Z.Q. Li, Structural and electrical transport properties of Nb-doped TiO 2 films deposited on LaAlO 3 by rf sputtering, Applied Surface Science 255(18) (2009) 8104-8109.

[26] T. Ishida, M. Okada, T. Tsuchiya, T. Murakami, M. Nakano, Structural and surface property study of sputter deposited transparent conductive Nb-doped titanium oxide films, Thin Solid Films 519(6) (2011) 1934-1942.
[27] S. Mukherjee, H. Becker, A.C. Bedini, A. Nebatti, C. Notthoff, D. Rogalla, S. Schipporeit, A. Soleimani-Esfahani, D. Mergel, Structural and electrical properties of Nb-doped TiO 2 films sputtered with plasma emission control, Thin Solid Films 568 (2014) 94-101.
[28] L. Mattheiss, Electronic structure of rhombohedral, Journal of Physics: Condensed Matter 8(33) (1996) 5987.
[29] N. Laidani, P. Cheyssac, J. Perrière, R. Bartali, G. Gottardi, I. Luciu, V. Micheli, Intrinsic defects and their influence on the chemical and optical properties of TiO2−xfilms, Journal of Physics D: Applied Physics 43(48) (2010) 485402.
[30] L. Gong, Y. Liu, X. Gu, J. Lu, J. Zhang, Z. Ye, Z. Chen, L. Li, Study on the thermal stability of Ga-doped ZnO thin film: A transparent conductive layer for dye-sensitized TiO 2 nanoparticles based solar cells, Materials Science in Semiconductor Processing 26 (2014) 276-281.
[31] K. Dib, R. Brahimi, Y. Bessekhouad, N. Tayebi, M. Trari, Structural, optical and transport properties of SxZnO, Materials Science in Semiconductor Processing 48 (2016) 52-59.
[32] M. Omar, F. Gorges, The optical energy gap dependence on both carrier concentration and intrinsic energy gap in n-type semiconductors, Materials Science in Semiconductor Processing 9(1) (2006) 164-167.
[33] M. Castro, L. Rebouta, P. Alpuim, M. Cerqueira, M. Benelmekki, C. Garcia, E. Alves, N. Barradas, E. Xuriguera, C. Tavares, Optimisation of surface treatments of TiO 2: Nb transparent conductive coatings by a post-hot-wire annealing in a reducing H 2 atmosphere, Thin Solid Films 550 (2014) 404-412.
[34] S.X. Zhang, D.C. Kundaliya, W. Yu, S. Dhar, S.Y. Young, L.G. Salamanca-Riba, S.B. Ogale, R.D. Vispute, T. Venkatesan, Niobium doped TiO[sub 2]: Intrinsic transparent metallic anatase versus highly resistive rutile phase, Journal of Applied Physics 102(1) (2007) 013701.
[35] J.Y. Yang, W.S. Li, H. Li, Y. Sun, R.F. Dou, C.M. Xiong, L. He, J.C. Nie, Grain size dependence of electrical and optical properties in Nb-doped anatase TiO2, Applied Physics Letters 95(21) (2009) 213105.